

www.acsami.org Research Article

Acrylic Films in Cosmetics: Decoding the Structural Mechanism of a **High-Performing Skin Coating**

Thi Q. Tran, Francesca Zuttion,* Veronique Valero, Simon Taupin, Romain Salva, Julien Portal, Gustavo S. Luengo,* and Philippe Leclère*



Cite This: ACS Appl. Mater. Interfaces 2025, 17, 59873-59883



ACCESS I

Metrics & More

Article Recommendations

Supporting Information

ABSTRACT: For the past two decades, petroleum-based polymers have dominated the long-wear makeup segment of the cosmetic industry. Film-forming agents, such as acrylic polymers, are highly valued for their versatility and their ability to create sebuminsensitive, elastic, and resilient films on the skin and thus remain widely used. However, current research is increasingly focused on identifying more eco-friendly and biodegradable alternatives. In this context, it is essential to analyze the properties of acrylic polymer films to elucidate the key characteristics that make these systems efficient in real-world applications. Here, macroscopic properties, such as tensile strength and tack, intrinsic parameters including glass transition temperature and particle size, as well as nanoscale structural, mechanical, and viscoelastic characteristics assessed



using Atomic Force Microscopy (AFM), are examined. This comprehensive analysis defines the requirements that future biodegradable alternatives must fulfill to replicate, or even surpass, the in vivo performance of traditional acrylics.

KEYWORDS: viscoelasticity, acrylate polymers, atomic force microscopy, nano-dynamic mechanical analysis, rheology

INTRODUCTION

During the last 20 years, the field of long-wear makeup for lipsticks and foundations has been dominated by petroleumbased solutions. Among these, acrylate polymers stand out for their remarkable versatility and broad applicability. Their inherent adhesive and film-forming properties, coupled with compatibility with a wide range of substrates, have positioned polyacrylates as a standard reference in cosmetics. 1,2 Serving as binders, emulsion stabilizers, absorbency enhancers, dispersants, and film-forming agents, these polymers contribute to transparent, durable, and pliable coatings in cosmetic formulations. Common acrylate monomers, such as n-butyl acrylate, methyl acrylate (MA), and ethyl acrylate (EA), are frequently copolymerized to tailor adhesive behavior by manipulating the glass transition temperature $(T_g)^{3-5}$ a key determinant of mechanical properties. 5-7 Adhesive properties along with resistance to skin sebum, which can cause plasticization of the coating and its cracking, confer good in vivo stability, and long-term performance.8 However, the limited biodegradability of acrylate polymers poses a growing concern.

In this study, a characterization of state-of-the-art acrylic polymers is performed, spanning from the macro- to the nanoscale, to elucidate their structure and properties in film coatings. Macroscopic techniques were used to evaluate different polymers characterized by varying the ratio of ethyl and methyl acrylate. The copolymer showing the best results in tensile and tack tests was further investigated at the nanoscale through simultaneous nanostructural, mechanical, and viscoelastic analysis using Atomic Force Microscopy (AFM), PeakForce Quantitative Nanomechanical Mapping (PF-QNM), and nanoDynamic Mechanical Analysis (AFMnDMA).10

While previous correlative approaches have mostly relied on macroscale tools like rheology and texture analysis for the characterization and classification of polymers and natural alternatives, 11,12 the use of AFM introduces nanoscale characterization of these materials. To date, cosmetic polymer characterization has primarily focused on topographic and elastic modulus analyses. 1,13 However, the application of AFMnDMA now enables the evaluation of the viscoelastic behavior of polymers, thereby providing a deeper understanding of filmforming capabilities. Numerous AFM-based viscoelastic modes have been developed and applied to the study of soft polymers, including off-resonance techniques such as AFM-nDMA, 14-

Received: July 4, 2025 Revised: September 15, 2025

Accepted: September 18, 2025 Published: October 16, 2025





photothermal (PT)-AFM nDMA, 18,19 and Fourier Transform (FT)-nDMA,²⁰ as well as on-resonance modes like multifrequency²¹ and nonlinear dynamic AFM.²² Given the important role of viscoelasticity not only in cosmetics but also in biological materials and other soft or elastic polymers, these advanced techniques are increasingly employed to achieve more accurate and detailed characterization of material physical properties. In cosmetics, the use of AFM enables the identification of optimal nanomechanical and viscoelastic properties of the coatings, ensuring a proper balance between adhesion and cohesion for long-lasting performance.

These results provide important information for the development of novel eco-friendly polymer-based materials with tailored viscoelastic properties. Characteristics exhibited by acrylate copolymers should be sought in next-generation sustainable film-formers to ensure durable in vivo performance, thereby paving the way for the development of more environmentally responsible cosmetic products.

■ MATERIALS AND METHODS

Commercial chemicals, including Stearyl Methacrylate, Methyl Acrylate, and Ethyl Acrylate, from Sigma-Aldrich were used as monomers for the synthesis of polymers. Tertbutyl peroxy-2ethylhexanoate (Trigonox T21S) was purchased from Akzo Nobel and used as a radical initiator. Isododecane (2,2,4,6,6-pentamethylheptane) was purchased from Ineos and directly used as the solvent throughout the experiments.

Polyacrylate Polymers Synthesis. The acrylate polymers 1,23 were synthesized in isododecane medium, maintained at a temperature of 90 °C under an argon atmosphere, with continuous stirring. The synthesis is schematized in Scheme 1. First, 60 g of isododecane,

Scheme 1. Reaction Scheme for Synthesis of Acrylic Copolymers^a



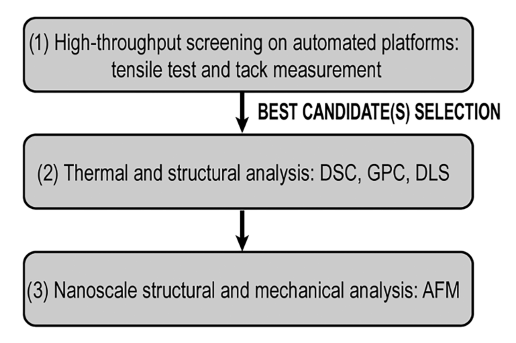
^aStep 1- Chain Initiation: The monomers and the initiator are added into isododecane solvent to start the polymerization for 2 h. Step 2-Chain-propagation: The polymer chains grow up for 7 h at 90 °C resulting in a milky solution. Step 3- Termination Chain: The final polymer solution consists of 50% solid content dispersed in isododecane.

13.75 g of stearyl methacrylate, 2.34 g of methyl acrylate, and 0.16 g of Trigonox 21S were placed in a reactor. After an initial 2-h reaction period, the reactor contents were supplemented with 2000 g of isododecane, followed by heating to 90 °C. In a second step (Scheme 1, Step 2), a mixture of 234 g of methyl acrylate, 234 g of isododecane, and 2.21 g of Trigonox 21S were introduced drop by drop for 1 h. This addition resulted in a milky appearance of the medium, which was left to react for a total of 7 h. To achieve a solid content of 50% by weight, 0.4 L of isododecane was introduced, followed by partial evaporation. Additionally, a dispersion of methyl acrylate particles stabilized through a statistical copolymer containing 85% (wt) stearyl methacrylate and 15% (wt) methyl acrylate in isododecane was successfully produced. The resulting poly(acrylate) dispersion encompassed a total composition of 94.5% (wt) methyl acrylate and 5.5% (wt) stearyl methacrylate, inclusive of both stabilizer and particles. In a similar protocol, varying amounts of ethyl acrylate (from 0 to 100%) were added (Scheme 1, Step 2)

instead of solely methyl acrylate monomers to modify the mixture

Polymer Characterization. Different in vitro techniques (Scheme 2) were applied to characterize the properties of the different

Scheme 2. Flow Chart of the Techniques Used to Study the Polymer Filmsa



^aTensile test and tack measurements are first intention analyses used to screen different compositions and select the most promising ones, based on mechanical and adhesion properties. The selected compositions are further analyzed, through Differential Scanning Calorimetry (DSC), Gel Permeation Chromatography (GPS) and Dynamic Light Scattering (DLS). Finally, nanoscale characterization is performed via Atomic Force Microscopy (AFM) to understand nanostructure, nanomechanical and viscoelastic properties.

copolymers and to select the best candidates for in vivo testing. Some of them are used as macroscopic, first intention screening techniques, while others have been employed only on selected conditions to better understand their properties.

Tensile Testing of Bulk Copolymers. Traction test was performed by following a standardized protocol on a Zwick machine without an extensometer. Films were prepared by depositing each studied polymer formulation on a Teflon plate and let them dry for 6 days under a hood with a controlled temperature and humidity (25 °C, 45%RH). The wet thickness of each film was 1.2 mm, while upon drying a thickness of 200–250 μ m was achieved and measured using a caliper. Dumbbell-shaped specimens were then cut with a punch to perform the traction tests. The distance between the jaws was 30 mm. The traction speed was 50 mm/min, and the sample was extended until a maximum length of 50 cm. A minimum of three samples per condition were tested. Stress-strain curves were obtained for each poly(acrylate) film. The mechanical properties at large strains and their fracture behaviors were studied using uniaxial elongation. The effective traction area, corresponding to the film surface loaded in tension, was $20 \times 4 \text{ mm}^2$.

Tack Measurements. Tack measurements were performed by following a standardized protocol in a customized automated platform for mechanical evaluation. These measurements allow to probe the stickiness of an adhesive coating. This is a measure of how fast a bond is formed when a surface is brought into contact with the adhesive material upon the application of a slight pressure. The poly(acrylate) solutions were deposited on both a Byko-chart (Byk ref. 2810) and an FP40 (Trellborg N4I01) substrates. Each polymer solution was diluted in isododecane at 20% and the deposited volume was calculated to obtain a dry-film thickness of 30-40 µm, after 24 h of drying under a hood with controlled temperature and humidity (25 °C and 45%RH). Byko-chart is a clear coated opacity chart for testing various coating properties, and copolymers dispersed in isododecane have good wettability on it. FP40 is an elastomeric substrate of butadiene-acrylonitrile copolymer containing diethylhexyl sebacate oil as a plasticizer. The plasticizer is released in the presence of isododecane and thus mimics the appearance of the sebum on the skin. If the polymer coating is sensitive to oil, then the diethylhexyl sebacate oil released by the FP40 substrate will increase the stickiness

Table 1. Compositions of Acrylate Polymers

Polymer mixtures	MA/EA ratio (w/w)	MA monomers (%wt)	EA monomers (%wt)	SMA monomers (%wt)	Isododeca ne (%wt)	Film- former aspect
0%EA	100/0	47	0	3	50	
10%EA	90/10	42.3	4.7	3	50	-
20%EA	80/20	37.6	9.4	3	50	-
50%EA	50/50	23.5	23.5	3	50	
100%EA	0/100	0	47	3	50	

of the film and result in higher tack values compared to those obtained on the Byko-chart substrate.

The interaction between the samples and a Viton spherical probe was studied. For each condition, five measurements were performed as follows: the probe was approached to the sample at a speed of 5 mm/s. Once the probe and the sample were in contact, the probe indented the sample up to a maximum applied force of 1 nN. The probe-sample contact was kept for 5 s (contact area: 1 mm²), and then the probe was retracted at a constant speed of 5 mm/s. Approach and retract force vs distance curves were obtained. The maximum registered force, defined as the tackiness of the system, was extracted from the retract curves to evaluate how strong the interaction between the polymer and the probe is.

Differential Scanning Calorimetry (DSC). Thermal analysis of the composites was analyzed by Differential Scanning Calorimetry using a DSC Q2000 from TA Instruments. The analysis was performed at 10 °C/min and a heat/cool/heat program was applied to each sample from -50 to 100 °C. The samples were prepared to weigh from 3 to 10 mg each in a standard $40~\mu\text{L}$ aluminum pan, with an empty $40~\mu\text{L}$ aluminum pan as reference.

Gel Permeation Chromatography (GPC). Gel Permeation Chromatography has been applied to characterize the molecular weight $(M_{\rm w})$ and molecular weight distributions $(M_{\rm w}/M_{\rm n})$ of the polymers under study. A Waters e2695 gel permeation chromatograph has been used. The instrument is composed of two columns: TSKgel α -3000/TSKgel α -5000 (Tosoh) of length 300 mm and internal diameter 7.5 mm and uses a Refractometer 2414 from Waters as detector. The temperature of the columns was maintained at 55 °C. The eluent was tetrahydrofuran (THF), and the flow rate was kept constant at 0.5 mL/min. A molecular weight calibration curve was produced using commercial polystyrene standards (PS-H (PL2010-0200)) from Agilent. Polymer solutions at approximately 0.5 wt % of active polymer in tetrahydrofuran were prepared and filtered through 0.45 μ m filters prior to injection.

Dynamic Light Scattering (DLS). The particle size of each acrylate polymer dispersion was characterized by dynamic light scattering. The particle sizing apparatus NANOZS from MALVERN was employed for the characterization. The samples were diluted

10,000 times in isododecane and pipetted into a plastic single-use cell (4 transparent faces, 1 cm side, and 4 mL capacity). The z-average hydrodynamic diameter (D) and size polydispersity factor (Q) measured in DLS were derived from the first cumulant of the cumulant fitting of the autocorrelation function.

Atomic Force Microscopy (AFM). Samples were prepared by applying 200 μ L of each acrylate polymer formulation to glass microscope slides. Slides were cleaned using 10% HCl followed by three rinses with Milli-Q water and dried using a stream of nitrogen. Subsequently, the samples were left to dry for 7 days in a fume hood to facilitate the evaporation of the isododecane solvent.

AFM analysis was performed at ambient conditions (room temperature and humidity) with a Dimension Icon AFM instrument from Bruker equipped with a Nanoscope V Controller. Topographical characterization was performed in tapping mode (AFM-TM) using RTESPA-300 cantilevers from Bruker, with a spring constant of $\sim\!42$ N/m and a nominal radius of curvature of $\sim\!10$ nm. Local mechanical and viscoelastic properties were investigated using the PeakForce-Quantitative Nanomechanical Mapping (PF-QNM) mode. Additionally, the recently developed AFM-nanoscale Dynamic Mechanical Analysis (AFM-nDMA) mode, combined with Fast Force Volume technique, 10,15,17 was employed using precalibrated RTESPA-300-30 cantilevers from Bruker. These tips have individually calibrated spring constant of 40 N/m and end radius of 30 nm (±15%). Tip parameters were obtained by scanning the QR code in the tip box.

Prior to each experiment, deflection sensitivity, PF-QNM and nDMA calibrations were performed on a sapphire substrate. A polystyrene sample with a known elastic modulus ($E \sim 3.2$ GPa) was then used to verify the tip radius at both the beginning and the end of the experiment, particularly if substantial changes in force curves or images were observed. Three different samples were studied, and on each sample, at least 3 random $100 \times 100~\mu\text{m}^2$ areas were analyzed. On each area, 3-5 PF-QNM images were acquired (image size: $10 \times 10, 5 \times 5$, and $2 \times 2~\mu\text{m}^2$) along with 15-20 nDMA curves. In PF-QNM mode, the applied force was set at 30 nN, while PeakForce frequency was fixed at 1 kHz and PeakForce amplitude was settled at 150 nm. With these experimental conditions, indentation was between 4 and 9 nm to ensure an elastic deformation regime. ²⁴ All

captured PeakForce images were recorded with a resolution of 256 × 256 data points at a sample rate of 0.3 Hz. In AFM-nDMA mode, the preloading force was 30 nN, the hold force was 10 nN, and the sweep in frequency between 1 and 200 Hz, using a randomized frequency sweep to mitigate the effects of resonant frequencies and minimize noise. Frequency sweeps were performed at specific locations, enabling the acquisition of force curves and subsequent plotting of E', E'', and $\tan \delta$ as a function of frequency. Additionally, a few spatially resolved maps of the rheological properties were generated at selected frequencies of 80 and 100 Hz.

Topographic images were analyzed with MountainsPremium v.10.3 software (DigitalSurf, Besançon, France) to reveal the morphological structure of the samples. Upon polynomial plane subtraction, roughness was calculated and particle analysis was performed using a threshold detection method. Curves obtained from PF-QNM nanomechanical images were fitted by the Johnson-Kendall-Roberts (JKR) model due to the strong adhesiveness of the sample under study. A software called pyCAROS (Python Code For Approach and Retract Force Curve Analysis on Organic and Hybrid Soft Materials), developed by the University of Mons, was used to establish the best fitting model for the obtained data. The software is written in Python and allows fitting PF-QNM force curves with various contact models (Hertz, 25 DMT, 26 JKR, 27 and Maugis-Dugdale, 28 Figure S1A). For each curve of the PF-QNM map, the quality of the fit is defined, based on the calculation of the R^2 parameter (Figure S1B) and the Tabor coefficient ^{29–31} (Figure S1C), with the Tabor coefficient determined individually for each curve in the image. This allows for the creation of a map that summarizes the most appropriate model for each recorded force curve. In the case of polyacrylate copolymers, the JKR model was deemed the most appropriate (Figure S1D). Elastic modulus maps were then generated from the JKR model fits, using the retract curve within the 10-90% contact region. More information about pyCAROS can be found in the SI.

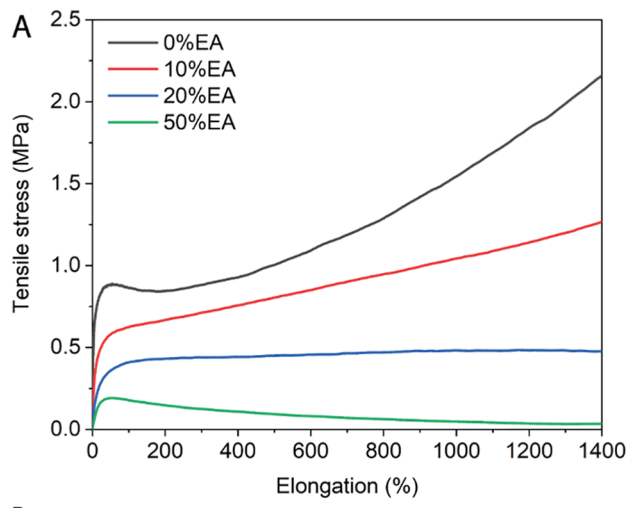
■ RESULTS AND DISCUSSION

In this study, a series of film-forming polymers with varying compositions of methyl acrylate (MA) and ethyl acrylate (EA) were screened to identify the best ratio for cosmetic applications. Table 1 presents the diverse acrylate polymer compositions investigated. Due to the low glass transition temperature of the EA polymer $(T_{\rm g} \sim -20~{\rm ^{\circ}C})$, $^{32-35}$ the 100% EA mixture failed to form a solid film (Table 1). This limitation underscores the crucial role of the EA concentration in achieving desirable film-forming properties.

Macroscopical analyses, namely, tensile stress and tack measurements were performed to assess resistance and adhesion of the film-formers.

Impact of Acrylate Composition on Macroscale Mechanical Performance: Tensile Stress and Tack **Measurements.** Polymers can exhibit glassy, brittle, elastic, or viscous behavior depending on the temperature and loading rate.³⁶ To evaluate the influence of the MA/EA ratio on the mechanical properties of polymer films, tensile stress experiments were conducted under controlled conditions (25 °C, 45%RH) and a constant elongation speed (50 mm/min). All acrylate polymers were evaluated except the 100%EA sample, which could not form a coherent film suitable for tensile analysis.

Stress-strain analysis reveals that 0%EA polymer forms the hardest film, followed by 10, 20, and 50%EA (Figure 1A and Table 2). All polymer films, except for 0%EA, display a linear regime in the plastic region: tensile stress either increases (10, 20%EA) or slightly decreases (50%EA) as elongation increases. Conversely, the 0%EA copolymer exhibits a constant or slightly decreasing tensile stress during the first 200% of elongation, followed by an abrupt increase until the maximum elongation



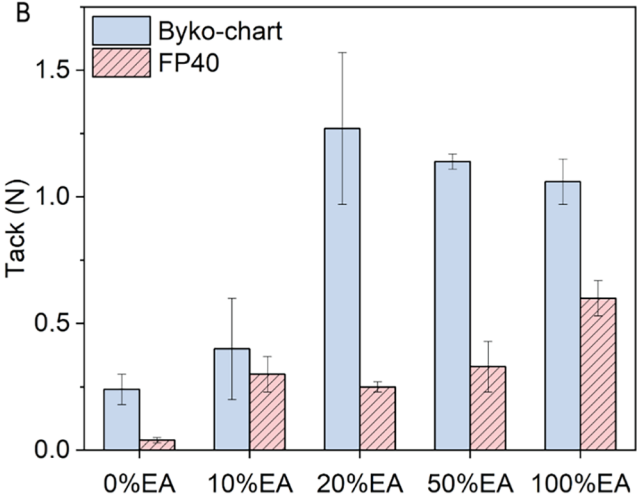


Figure 1. (A) Tensile stress as a function of elongation of poly(acrylate) polymer mixtures from 0 to 50%EA. (B) Tack measurements for the different poly(acrylate) mixtures. Measurements were performed on two substrates: the neutral Byko-chart (blue histograms) and the FP40 (light red, dashed). Values are presented as mean ± standard deviation.

Table 2. Mechanical Properties of Polymer Mixtures^a

Polymer mixtures	E (MPa)	$\sigma_{ m max}~({ m MPa})$	σ (MPa)	ε (%)
0%EA	41 ± 2	2.4 ± 0.1	no break	>1500
10%EA	14 ± 1	1.4 ± 0.2	no break	>1500
20%EA	7 ± 2	0.55 ± 0.06	no break	>1500
50%EA	2.2 ± 0.2	0.18 ± 0.05	no break	>1500

^aElastic modulus (E), maximum tensile stress ($\sigma_{ ext{max}}$), tensile stress at break (σ) , and elongation at break (ε) of the different mixtures. Values are (mean ± standard deviation).

is reached. This behavior is characteristic of a glassy or semicrystalline state,³⁷ and further thermal analysis will be performed to clarify its physical state. The observed trend can be attributed to the effect of side chain length on polymer flexibility.³⁸ The 0%EA polymer, composed almost entirely of methyl acrylate monomers with short COOCH₃ side chains, results in an oriented amorphous structure.

In contrast to the 0%EA polymer, the 10, 20, and 50%EA polymers exhibit a range of mechanical behaviors, becoming progressively less elastic and more viscous with increasing EA content. The incorporation of EA monomers disrupts the

orientation and arrangement of the polymer chains, increasing structural disorder and leading to the decline in both the elastic modulus and tensile stress. In the plastic region, only the 50% EA polymer film shows a steady flow regime, where tensile stress decreases with increasing elongation, making it promising for use as a film-former for cosmetic coatings.

While the 0, 10, and 20%EA mixtures have properties similar to previously described nonaqueous polymer dispersions (NAD), the 50%EA exhibits higher viscosity and lower elastic modulus compared to NAD. Notably, the 50%EA film shows significant reduction in both fracture stress and strain compared to its counterparts (Table 2). This composition also presents a much lower elastic modulus, registering a 20-fold decrease compared with the 0%EA sample. Furthermore, the maximum tensile stress achieved by the 0%EA polymer (2.4 MPa) exceeds that of the 50%EA composition (0.18 MPa) by a factor of 12. Interestingly, even at 100% elongation, the 50%EA polymer reaches a tensile stress of only approximately 0.2 MPa.

While mechanical integrity is critical for cohesion, adhesion performance is essential for cosmetic applications. To this end, the tackiness of all acrylate polymer formulations (0–100% EA) was evaluated following isododecane evaporation. As previously described, measurements were performed on both a Byko-chart and FP40 substrates. The use of both substrates enables assessment of whether the polymer film can be plasticized by oil, mimicking the effect of skin sebum in *in vivo* conditions. If tack values are higher on FP40 compared to Byko-chart, the polymer is likely plasticized by skin sebum during *in vivo* application, leading to product migration and an undesirable sticky sensation.³⁹

Figure 1B summarizes the tack measurements, highlighting the relationship between the EA concentration and tack. On the Byko-chart substrate, tackiness increased from 0.24 \pm 0.06 N for 0%EA up to 1.27 \pm 0.3 N at 20%EA, before slightly decreasing to 1.14 \pm 0.03 N at 50%EA and settling at 1.06 \pm 0.09 N for 100%EA. It is important to note that at 100%EA content, the polymer does not form a coherent film: it mostly behaves as an adherent viscous liquid. Consequently, tack measured on the FP40 elastomer is higher for this condition compared to all other samples. Therefore, sebum is not a plasticizer for these films, in contrast to NAD polymers. 1

Combined mechanical and tack analyses establish a correlation between EA concentration and adhesive properties in acrylate polymer film-formers. Optimizing these parameters is crucial for enhancing skin adhesion in cosmetic formulations and achieving good *in vivo* performance. The final coating must be soft and flexible, free from internal stress and tension, and remain continuous without cracking during facial movement. Description of the continuous without cracking during facial movement.

Based on this analysis, the 50%EA polymer emerges as the most promising candidate for long-lasting skin adhesion. This optimal formulation exhibits: (1) an elastic modulus (2.2 MPa) closely matching that of the stratum corneum, the outermost skin layer, ^{39,40} ensuring comfortable wear; ² (2) favorable tack properties indicative of enhanced skin adhesion; and (3) moderate tack on FP40 elastomer, suggesting controlled sensitivity to sebum. *In vivo* tests confirmed this hypothesis, demonstrating that the 50%EA coating remained homogeneous and free of cracks after 3 days of application, in contrast to the 0 and 20%EA dispersions (Figure S4).

Accordingly, the 50%EA polymer was selected for further analysis. Several analytical techniques, including DSC, GPC,

DLS, and AFM, were employed to further investigate its molecular, thermal, and nanoscale properties and to better understand the interactions between the two main components

Physical Properties of 50%EA Polymer. Molecular Weight and Size - GPC and DLS Analyses. To gain a comprehensive understanding of the 50%EA polymer, multiple characterization techniques were employed. GPC analysis revealed a weight-average molecular weight $(M_{\rm w})$ of 115,800 Da and a number-average molecular weight $(M_{\rm n})$ of 8400 Da. The resulting polydispersity index (PI) of approximately 13 indicates an extremely broad molecular weight distribution, which might be attributed to the two-step uncontrolled free-radical polymerization synthesis process at high temperatures. Free radicals become more active with increasing temperature, leading to a higher probability of chain combination or an increased termination rate. 41,42

DLS measurements, performed on a 10,000-fold dilution in isododecane, provided insights into the polymer's size in solution. Application of the Stokes–Einstein relation was used to determine a hydrodynamic diameter (D) of 200 nm and a polydispersity factor (Q) of 0.5 for the 50%EA polymer. The observed D value suggests that multiple acrylate polymer chains aggregate and overlap, forming microparticles in the isododecane solvent.

Glass Transition Temperature and Monomer Miscibility - DSC. DSC is a powerful tool for probing the physical state and potential phase separation in heterogeneous polymers. A single glass transition temperature ($T_{\rm g}$) often indicates homogeneous polymer chains with randomly distributed monomers. For example, polymethyl acrylate (PMA) homopolymer exhibits a single glass transition temperature with a $T_{\rm g}$ ranging from 8 to 55 °C depending on molecular weight, $^{43-45}$ implying that its physical state at room temperature can be either glassy or rubbery.

Figure 2 displays the DSC thermograms for both the 0 and 50%EA polymers between -50 and 100 °C. Acrylate adhesives can withstand brief exposures up to 177 °C, 46,47 ensuring copolymer stability during DSC analysis. The acrylic polymer containing only methyl acrylate in the core (0%EA) was studied as a reference system. It shows a single transition

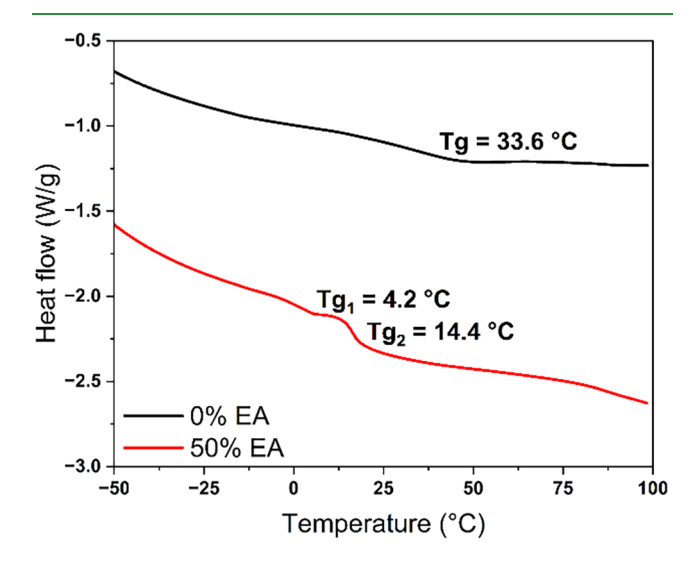


Figure 2. DSC thermogram for the 0 and 50%EA polymers in the temperature range of -50 to 100 °C.

temperature at 33.6 °C, indicating that this compound is miscible and no phase separation is observed. Using the Fox equation (see SI), the $T_{\rm g}$ estimation is from -0.4 to 18 °C, which is lower than the experimentally observed $T_{\rm g}$. The increase in T_g compared to the theoretical value could be due to side reactions, such as backbiting and β -scission, which may occur during the free-radical polymerization of methyl acrylate. Polyethyl acrylate itself has a T_{σ} of about -20°C. 45,50 Given the high EA content (around 50% by weight) in the 50%EA copolymer, the $T_{\rm g}$ of the EA-rich phase is expected to be below room temperature, with a theoretical T_g value of -5.6 °C as estimated by the Fox equation. As expected, the addition of ethyl acrylate results in a reduction of the overall glass transition temperature of the copolymer, with observed values at 4.2 and 14.4 °C. The presence of two transition temperatures indicates phase separation, suggesting structural heterogeneity, which is common in free-radical copolymerization of two distinct monomers. Lowering the $T_{\rm g}$ could be desirable for cosmetic (adhesive) applications, as it could enhance melt behavior and spreadability on the skin.

Nanoscale Morphological and Mechanical Characterization - AFM. Microstructure and Self-Assembly of Copolymers: AFM Tapping Mode Analysis. AFM is a powerful tool for characterizing nanoscale film roughness, nanomechanical properties, and even viscoelastic behavior. In this study, multiple AFM modes were employed to characterize the properties of the 50%EA polymer with the aim of understanding its nanoscale behavior and correlating these findings with macroscale analysis and, ultimately, in vivo performances.

A first analysis of the polymer nanostructure was performed by using TM-AFM with a sharp tip. This mode is frequently used to probe the microstructure of phase-separated polymers, $^{51-53}$ such as the PMMA-b-PIOA-b-PMMA triblock copolymers studied by Tong et al. 53 In their study, TM-AFM images showed a two-phase separation of the triblock copolymers, confirming suspicions raised by DSC and DMTA. 53 In the case of the 50%EA copolymer, while the polymerization strategy was designed to yield a miscible, single-phase polymer, the presence of two distinct $T_{\rm g}$ values in the DSC results suggested potential phase separation within the copolymer. TM-AFM analysis, as depicted in Figure 3, confirmed this hypothesis, revealing an obvious two-phase microstructure, as evidenced in the phase image (Figure 3B).

The 50%EA copolymer exhibits a particle-like morphology with features of varying sizes. Particle analysis determined the mean diameter of these structures, ranging from 100 nm to 1.5 μ m (Figure 3C). This surface texture contributed to a root-mean-square roughness (RMS) of 4.3 \pm 1.6 nm calculated on images of 5 \times 5 μ m², indicating a relatively rough surface compared to NAD dispersions, where the calculated RMS on 5 \times 5 μ m² images was below 3 nm. ¹

Phase imaging (Figure 3B) exhibited a two-phase contrast distribution, indicative of varying material rigidity within the sample, with brighter regions corresponding to harder materials and darker regions corresponding to softer ones. While AFM-TM provides a qualitative assessment of mechanical property variations, ¹³ it lacks the capability for precise quantification. Therefore, quantitative AFM mechanical modes were used for a more precise characterization. Specifically, AFM PF-QNM and nDMA modes were employed to obtain quantitative measurements of rigidity (e.g., elastic modulus), adhesion, and viscoelasticity of the 50%EA polymer.

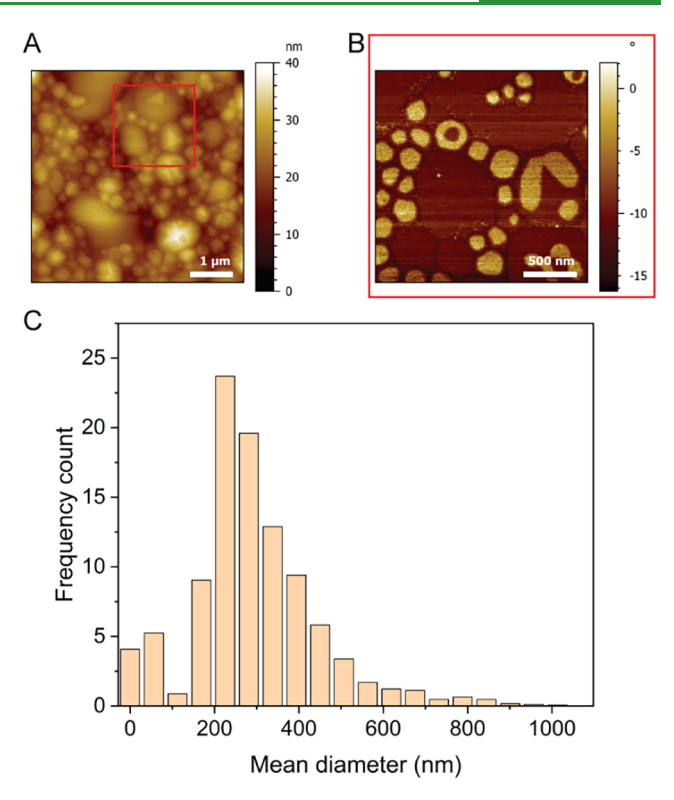


Figure 3. (A) TM-AFM $5 \times 5 \ \mu m^2$ topographic image of the 50%EA polymer. The red square shows the region of the $2 \times 2 \ \mu m^2$ image presented in part (B). (B) Phase characteristic image of 50%EA polymer. Image size: $2 \times 2 \ \mu m^2$. (C) Mean diameter distribution obtained from particle analysis over all of the analyzed images (10 images of $5 \times 5 \ \mu m^2$).

Nanomechanical Properties: AFM PF-QNM Analysis. Atomic Force Microscopy using PeakForce-Quantitative Nanomechanical Mapping (PF-QNM) was first employed to obtain quantitative measurements of the rigidity and adhesion of the 50%EA polymer.

As depicted in Figure 4A, PF-QNM topographic images of the 50%EA polymer exhibit a particle-like structure with assemblies of varying sizes, consistent with AFM-TM observations (Figure 3). Mechanical mapping of the elastic modulus (Figure 4B) reveals the presence of both softer and harder regions within the sample, which are further categorized into three distinct clusters (Figures S1-S3), with average elastic modulus values (±standard deviations, calculated from five $10 \times 10 \ \mu\text{m}^2$ images) of $379 \pm 71 \ \text{MPa}$ (hardest), $272 \pm 71 \ \text{MPa}$ 50 MPa (intermediate), and 181 ± 22 MPa (softest). The hardest cluster likely corresponds to MA-rich structures, while the intermediate modulus cluster is attributed to EA-rich regions. The softest cluster, located at the boundaries between particles, may be influenced by edge effects due to the curved nature of the surrounding polymer and the finite size of the AFM tip. This region potentially associated with a mixture of EA and SMA components was excluded from further analysis. Nanoscale PF-QNM elastic modulus is 2 orders of magnitude higher than what obtained with a macroscopic tensile test. Several factors may influence nanomechanical measurements on soft polymers, including adhesion, model selection, and experimental factors.⁵⁴ In this case, the choice of a small tip radius ($r \sim 30$ nm) could induce an overestimation of the elastic modulus, while allowing high-resolution imaging that reveals the heterogeneity and phase separation of the acrylic

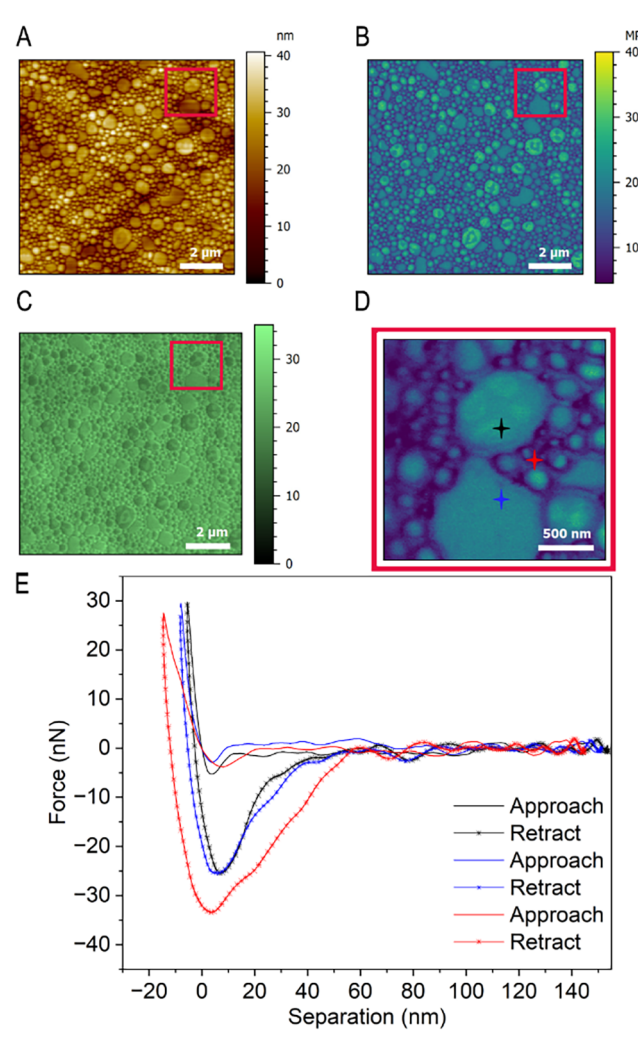


Figure 4. PF-QNM characterization of the 50%EA: characteristic maps of the (A) topography, (B) elastic modulus, and (C) adhesion of the sample are presented (image size $10\times10~\mu\text{m}^2$, $256\times256~\text{pxl}$). (D) High-resolution map of the elastic modulus for the region indicated by the red box in images (A–C). (E) Representative PF-QNM force—distance curves corresponding to the regions marked with stars in part (D).

compounds within the polymer structure. Furthermore, the 1 kHz frequency used for nanoscale measurements may also contribute to discrepancies between bulk and AFM PF-QNM results. Due to the short interaction time between the tip and the sample, the polymer response is predominantly elastic,³⁶ while in tensile tests, the longer loading rate (50 mm/min) allows for polymer chains realignment. Thus, 50%EA polymer exhibits more viscous (softer) behavior in tensile tests than in PF-QNM measurements. To further investigate the impact of frequency on mechanical properties, AFM-nDMA analysis was conducted to elucidate the viscoelastic behavior of the 50%EA film; these results are discussed in the following section.

Similarly to the elastic modulus, three main adhesion behaviors were identified and clearly distinguished in the retraction curves shown in Figure 4E. The harder mechanical regions are the least adhesive (average adhesion force $F_{\rm a} \sim 10$ nN, corresponding to the region marked by a black star in Figure 4C and illustrated by the black approach/retract curves in Figure 4D); intermediate regions are characterized by an average adhesion force of $F_{\rm a} \sim 17$ nN (blue star in Figure 4C

and blue curves in Figure 4D), while the softer mechanical regions exhibit the highest adhesion force ($F_a \sim 25$ nN, red star in Figure 4C and red curves in Figure 4D), primarily found at the boundaries between particles. The values obtained can be discussed in comparison to the macroscopic tack parameter by considering the force-to-probe radius ratio (F/r). As with the elastic modulus, a 2 orders of magnitude difference is observed between macroscale and nanoscale measurements. For tack tests on Byko chart, the F/r ratio is 2.7 N/mm (using a Viton probe of radius 0.56 mm), whereas PF-QNM measurements yield an average F/r ratio of 450 N/mm. Differences in contact time (5 s in tack measurement versus a few milliseconds for PF-QNM), as well as probe material and the viscoelastic nature of the sample, likely contribute to this discrepancy.

Viscoelastic Properties: AFM-nDMA Analysis. Neither PF-QNM nor tensile testing alone can fully elucidate the viscoelastic behavior of soft polymers at the nanoscale. Therefore, the recently developed AFM-nDMA mode was employed to investigate the complex mechanical response of the 50%EA polymer.

AFM-nDMA data were acquired as both maps at a single frequency and curves from frequency sweeps between 1 and 200 Hz. Although AFM-nDMA provides lower spatial resolution than PF-QNM (nDMA: 78 nm/pixel versus PF-QNM: 39 nm/pixel), the topography images consistently reveal the particle-like features observed in AFM-TM and PF-QNM. From the AFM-nDMA measurements, maps of adhesion force, elastic modulus, storage modulus (E'), loss modulus (E''), and loss tangent $(\tan \delta)$ were calculated (Figure 5A-F). The adhesion force was observed to be approximately 30 nN, similar to values obtained with PF-QNM, while the elastic modulus was approximately 1 MPa. This value is significantly lower (approximately 2 orders of magnitude) than that obtained via PF-QNM ($E \sim 227$ MPa), and it is closer to the value observed in bulk measurements ($E \sim 2.2$ MPa). This discrepancy likely results from the intrinsic viscoelastic nature of the sample and the different loading rates used in these techniques. The frequency rate in AFM-nDMA is approximately between 10 and 10³ times slower than in PF-QNM (1 kHz in PF-QNM, between 1 and 200 Hz in nDMA), which influences the measured mechanical response. In contrast, the adhesion force measured by AFM-nDMA (~30 nN at 80 Hz; Figure 5C) is comparable to that obtained previously. The AFM-nDMA-derived rheological maps at 80 Hz further highlight the heterogeneous nature of the sample. Regions exhibiting higher elasticity (lighter regions in the E' map, Figure 5D) also display elevated viscous behavior (pink/blue zones in the E'' map, Figure 5E), with E' and E'' values around 3 and 5 MPa, respectively. The surrounding areas appear less responsive to the dynamic mechanical stimulation. The tan δ map (Figure 5F) exhibits values near unity, indicating predominantly viscous behavior for the polymer, with an average value of approximately 1.5. The blue points observed in the $\tan\delta$ map are likely artifacts associated with the sample topography, as they primarily correspond to the edges of the particle-like structures.

Frequency sweep measurements reveal storage modulus values ranging from 3 to 25 MPa and loss modulus values ranging from 2 to 60 MPa for the 50%EA polymer (Figure 6). The similarity between E' and E'', particularly at lower frequencies, suggests a comparable contribution of elastic and viscous components to the material's mechanical response. Furthermore, the loss tangent value lies within the range of 0.5

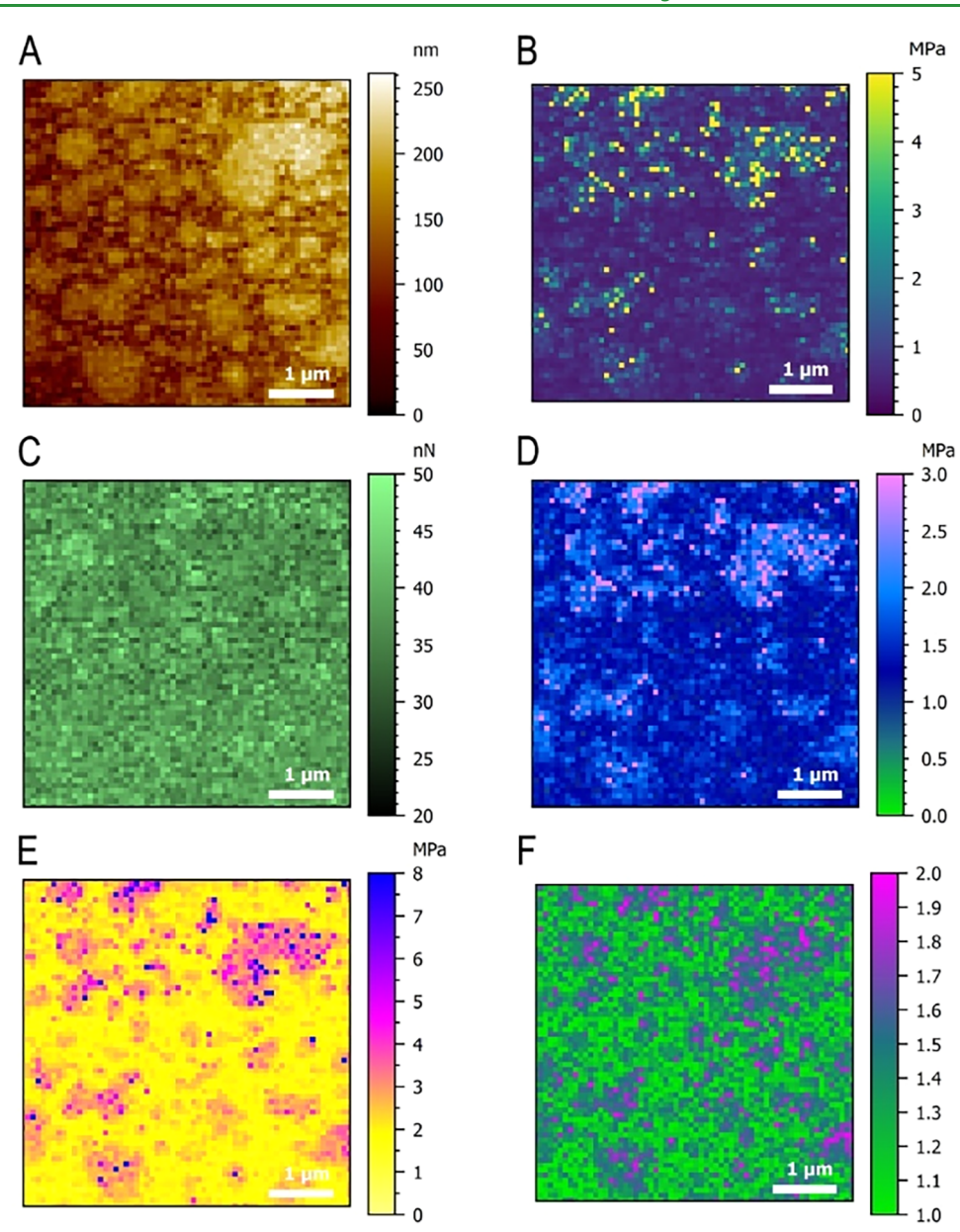


Figure 5. AFM-nDMA analysis of the 50%EA sample. Images at a single frequency (80 Hz at $5 \times 5 \mu \text{m}^2$). (A) Topography, (B) elastic modulus, (C) adhesion, (D) storage modulus, (E) loss modulus, and (F) loss tangent.

to 1 in the low-frequency band (1–20 Hz), corresponding to a semiliquid state; while at frequencies above 20 Hz, the $\tan\delta$ value exceeds 1, indicating the liquid-like state of the material (Figure 6). These rheological characteristics indicate a semiliquid state for the 50%EA polymer at low frequency, which aligns well with the desired properties of an adhesive material for cosmetic applications, facilitating ease of spreading on various substrates.

CONCLUSIONS

Macro-to-nanoscale physical property measurements identify the 50%EA formulation as the optimal cosmetic film-former. Macroscale analysis revealed a strong correlation between EA concentration and adhesive properties, with the 50%EA polymer exhibiting an elastic modulus comparable to that of the stratum corneum⁸ and enhanced adhesion compared to the 0%EA polymer. While these techniques elucidate bulk properties of a 200–250 μ m thick film, nanoscale measure-

ments using AFM enabled the investigation of much thinner films, on the order of several hundred nanometers. The combined information on topography, modulus, and adhesion within the same region provides a deeper understanding of the microstructure, arrangement, and phase separation of the copolymer. AFM revealed the particle-like structure and the existence of a nanomechanical heterogeneity within the system. The use of AFM clarified the key characteristics required for the optimal ratio of methyl acrylate and ethyl acrylate to achieve a high performance. Similar nanoscale properties, especially in terms of viscoelastic behavior, can be anticipated in future eco-friendly polymer solutions.

This study demonstrates how combining macro- and nanoscale techniques enables a comprehensive understanding of the physical properties, particularly the adhesive and viscoelastic behavior, of soft polymers. This methodology enables quantitative exploration that can be extended to other cosmetic polymers and new material families. It also holds

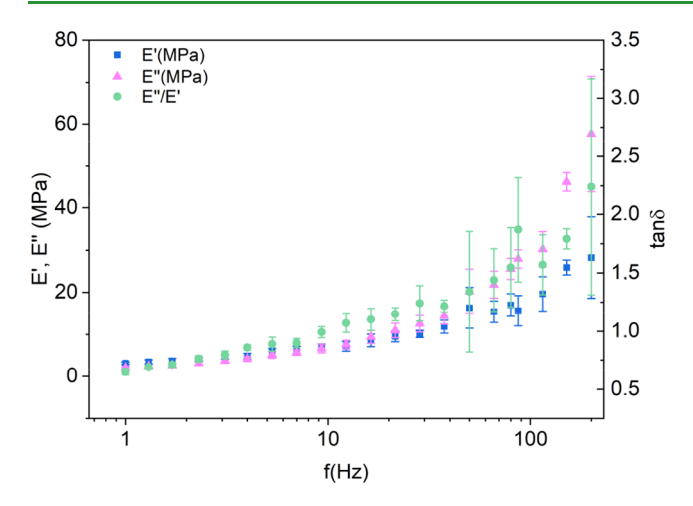


Figure 6. Representation of the E' (blue), E'' (pink), and $\tan \delta$ (green) as a function of the frequency (mean value \pm standard deviation). Frequency sweep from 1 to 200 Hz.

significant potential for broad adoption in related fields such as painting, coatings, adhesives, and textiles.

In future work, an example of the polyester family, the poly(3-hydroxynonanoate), will be investigated^{55,56} and discussed in the light of the present findings. This class of polymers offers greater potential to reduce environmental impact, especially in terms of biodegradability,⁵⁷ while ensuring a high degree of design flexibility to achieve the desired level of cosmetic performance. Finally, this study provides an initial insight into AFM capabilities in the field of cosmetic polymers research. AFM's versatility establishes a framework for new experimental designs that can more closely mimic *in vivo* situations, including sample preparation and external conditions such as temperature and relative humidity, which are under development.

ASSOCIATED CONTENT

Supporting Information

The Supporting Information is available free of charge at https://pubs.acs.org/doi/10.1021/acsami.5c13170.

Fox equation; explanation of PyCAROS software, and examples of obtained results; *in vivo* test comparison of acrylate copolymers performances (PDF)

AUTHOR INFORMATION

Corresponding Authors

Francesca Zuttion — L'Oréal Advanced Research Centre, 93600 Aulnay-sous-Bois, France; orcid.org/0000-0001-5496-1016; Email: francesca.zuttion@loreal.com

Gustavo S. Luengo – L'Oréal Advanced Research Centre, 93600 Aulnay-sous-Bois, France; ⊚ orcid.org/0000-0001-8816-5536; Email: gustavo.luengo@loreal.com

Philippe Leclère — Laboratory for Physics of Nanomaterials and Energy (LPNE), Department of Physics, Materials Science and Engineering Research Institute, University of Mons (UMONS), B-7000 Mons, Belgium; orcid.org/0000-0002-5490-0608; Email: philippe.leclere@umons.ac.be

Authors

Thi Q. Tran – Laboratory for Physics of Nanomaterials and Energy (LPNE), Department of Physics, Materials Science and Engineering Research Institute, University of Mons (UMONS), B-7000 Mons, Belgium; Present Address: Institute of Physical Chemistry - Paris-Saclay University, 91400 Orsay, Essonne, France

Veronique Valero – L'Oréal Advanced Research Centre, 93600 Aulnay-sous-Bois, France

Simon Taupin – L'Oréal Advanced Research Centre, 93600 Aulnay-sous-Bois, France

Romain Salva – L'Oréal Advanced Research Centre, 93600 Aulnay-sous-Bois, France

Julien Portal – L'Oréal Advanced Research Centre, 93600 Aulnay-sous-Bois, France

Complete contact information is available at: https://pubs.acs.org/10.1021/acsami.5c13170

Author Contributions

F.Z., P.L., G.S.L., and J.P. conceived the AFM experiments. J.P. and V.V. conceived the macroscale evaluations (tensile test, track measurements, etc.). S.T. synthesized the polymers. V.V. performed tensile test, tack measurements, and analyzed the related data. R.S. performed DLS and GPC experiments and analyzed the related data. T.Q.T. performed DSC and AFM experiments and analyzed the related data. T.Q.T., F.Z., P.L., J.P., V.V., and G.S.L. data discussion. T.Q.T. and F.Z. writing—original draft preparation. F.Z. writing—reviewing and editing. J.P. and P.L. project administration. All authors have given approval to the final version of the manuscript.

Notes

The authors declare the following competing financial interest(s): F.Z, V.V., S.T., R.S., J.P., and G.S.L. are employees of LOREAL engaged in research activities. P.L. and T.T.Q. received partial funding from LOREAL for this project.

ACKNOWLEDGMENTS

P.L. research at LPNE (UMONS) is partly supported by F.R.S. FNRS (Belgium) via the Grands Equipments Project (40007941) – 2022 "Interuniversity Platform for the Analysis of the Nanoscale Properties of Emerging Materials and their Applications (IPANEMA)". T.Q.T. thanks Communauté française de Belgique—Actions de Recherche Concertées, via the ARC project MecaRiboSynth (ARC No ARC-19/23 UMONS4) for her Ph.D. grant. The authors thank François Fievet and Kilian Bertrand for their contribution in the development of PyCAROS.

REFERENCES

- (1) Portal, J.; Schultze, X.; Taupin, S.; Arnaud-Roux, M.; Bonnard, J.; Naudin, G.; Hely, M.; Bui, H.; Biderman, N. Adhesion Aspect and Film-Forming Properties of Hydrocarbon Polymers-Based Lipsticks. In Surface Science and Adhesion in Cosmetics; Wiley, 2021; pp 451–486
- (2) Luengo, G. S.; Bui, H. S.; Portal, J. Formation and Performance of Cosmetic Films in Cosmetics. In *Handbook of Cosmetic Science and Technology*; CRC Press, 2023; pp 167–181.
- (3) Maassen, W.; Meier, M. A. R.; Willenbacher, N. Unique Adhesive Properties of Pressure Sensitive Adhesives from Plant Oils. *Int. J. Adhes. Adhes.* **2016**, *64*, 65–71.
- (4) Ito, K.; Usami, N.; Yamashita, Y. Syntheses of Methyl Methacrylate-Stearyl Methacrylate Graft Copolymers and Characterization by Inverse Gas Chromatography. *Macromolecules* **1980**, *13* (2), 216–221.
- (5) Abo-Shosha, M. H.; Ibrahim, N. A.; Allam, E.; El-Zairy, E. Preparation and Characterization of Polyacrylic Acid/Karaya Gum

- and Polyacrylic Acid/Tamarind Seed Gum Adducts and Utilization in Textile Printing. *Carbohydr. Polym.* **2008**, 74 (2), 241–249.
- (6) Safa, K. D.; Babazadeh, M. Glass Transition Temperature Modification of Acrylic and Dienic Type Copolymers of 4-Chloromethyl Styrene with Incorporation of (Me 3Si)3C- Groups. *Eur. Polym. J.* **2004**, 40 (8), 1659–1669.
- (7) Anastasio, R.; Cardinaels, R.; Peters, G. W. M.; van Breemen, L. C. A. Structure–Mechanical Property Relationships in Acrylate Networks. *J. Appl. Polym. Sci.* **2020**, *137* (13), No. 48498, DOI: 10.1002/app.48498.
- (8) Bui, H. S.; Coleman-Nally, D. Film-Forming Technology and Skin Adhesion in Long-Wear Cosmetics. In *Adhesion in Pharmaceutical, Biomedical and Dental Fields*, 2017; pp 141–166.
- (9) Pittenger, B.; Erina, N.; Su, C. Mechanical Property Mapping at the Nanoscale Using PeakForce QNM Scanning Probe Technique. In *Nanomechanical Analysis of High Performance Materials*; Tiwari, A., Ed.; Solid Mechanics and Its Applications; Springer: Dordrecht, 2014; Vol. 203, pp 31–51.
- (10) Pittenger, B.; Osechinskiy, S.; Yablon, D.; Mueller, T. Nanoscale DMA with the Atomic Force Microscope: A New Method for Measuring Viscoelastic Properties of Nanostructured Polymer Materials. *JOM* **2019**, *71* (10), 3390–3398.
- (11) Tafuro, G.; Costantini, A.; Baratto, G.; Francescato, S.; Semenzato, A. Evaluating Natural Alternatives to Synthetic Acrylic Polymers: Rheological and Texture Analyses of Polymeric Water Dispersions. ACS Omega 2020, 5 (25), 15280–15289.
- (12) Tafuro, G.; Costantini, A.; Baratto, G.; Busata, L.; Semenzato, A. Rheological and Textural Characterization of Acrylic Polymer Water Dispersions for Cosmetic Use. *Ind. Eng. Chem. Res.* **2019**, *58* (51), 23549–23558.
- (13) Couderc, S.; Hanzawa, M.; Ibe, Y.; Miyamoto, M.; Courtois, A.; Thollas, B.; Guarilloff, P.; Ogura, T. Polyhydroxyalkanoate Heteropolymer as a New Biodegradable Film-Forming Agent for a Highly Sebum-Resistant Silicone-Free Fluid Foundation. *IFSCC Mag.* **2024**, 27 (27), 147–155.
- (14) Yang, L.; Nickmilder, P.; Verhoogt, H.; Hoeks, T.; Leclère, P. Probing Viscoelastic Properties and Interfaces in High-Density Polyethylene Vitrimers at the Nanoscale Using Dynamic Mode Atomic Force Microscopy. ACS Appl. Mater. Interfaces 2024, 16 (29), 38501–38510.
- (15) Tilbury, M. A.; Tran, T. Q.; Shingare, D.; Lefevre, M.; Power, A. M.; Leclère, P.; Wall, J. G. Self-Assembly of a Barnacle Cement Protein into Intertwined Amyloid Fibres and Determination of Their Adhesive and Viscoelastic Properties. J. R. Soc. Interface 2023, 20 (205), No. 20230332, DOI: 10.1098/rsif.2023.0332.
- (16) Lefevre, M.; Tran, T. Q.; De Muijlder, T.; Pittenger, B.; Flammang, P.; Hennebert, E.; Leclère, P. On the Nanomechanical and Viscoelastic Properties of Coatings Made of Recombinant Sea Star Adhesive Proteins. *Front. Mech. Eng.* **2021**, 7 (May), No. 667491.
- (17) Nguyen, H. K.; Shundo, A.; Ito, M.; Pittenger, B.; Yamamoto, S.; Tanaka, K.; Nakajima, K. Insights into Mechanical Dynamics of Nanoscale Interfaces in Epoxy Composites Using Nanorheology Atomic Force Microscopy. ACS Appl. Mater. Interfaces 2023, 15 (31), 38029–38038.
- (18) Piacenti, A. R.; Adam, C.; Hawkins, N.; Wagner, R.; Seifert, J.; Taniguchi, Y.; Proksch, R.; Contera, S. Nanoscale Rheology: Dynamic Mechanical Analysis over a Broad and Continuous Frequency Range Using Photothermal Actuation Atomic Force Microscopy. *Macromolecules* **2024**, *57* (3), 1118–1127.
- (19) Adam, C. E.; Piacenti, A. R.; Zhang, Y.; Waters, S. L.; Contera, S. Viscoelastic Time Responses of Polymeric Cell Substrates Measured Continuously from 0.1–5,000 Hz in Liquid by Photothermal AFM Nanorheology. *Nanoscale* **2025**, *17*, 21810–21836.
- (20) Dokukin, M.; Sokolov, I. High-Resolution High-Speed Dynamic Mechanical Spectroscopy of Cells and Other Soft Materials with the Help of Atomic Force Microscopy. *Sci. Rep.* **2015**, *5* (July), No. 12630, DOI: 10.1038/srep12630.
- (21) Garcia, R.; Herruzo, E. T. The Emergence of Multifrequency Force Microscopy. *Nat. Nanotechnol.* **2012**, 7 (4), 217–226.

- (22) Fricke, L. V.; Wansink, N.; Rosso, M.; Staufer, U.; Belardinelli, P.; Alijani, F. Probing Viscoelasticity of Polymeric Coatings Using Nonlinear Dynamic Atomic Force Microscopy. *Small Methods* **2025**, No. 2500723.
- (23) Patil, A.; Sandewicz, R. W. Cosmetic Science and Polymer Chemistry: Perfect Together. In *Polymers for Personal Care and Cosmetics*, ACS Symposium Series; American Chemical Society, 2013; Vol. 1148, pp 13–37.
- (24) Chyasnavichyus, M.; Young, S. L.; Tsukruk, V. V. Probing of Polymer Surfaces in the Viscoelastic Regime. *Langmuir* **2014**, *30* (35), 10566–10582.
- (25) Lacaria, L.; Podestà, A.; Radmacher, M.; Rico, F. Contact Mechanics. In *Mechanics of Cells and Tissues in Diseases: Biomedical Methods: Volume 1*, hal-04761046f, 2023; Vol. 1, pp 21–64.
- (26) Derjaguin, B. V.; Muller, V. M.; Toporov, Y. P. Effect of Contact Deformations on the Adhesion of Particles. *J. Colloid Interface Sci.* 1975, 53 (2), 314–326.
- (27) Johnson, K. L.; Kendall, K.; Roberts, A. D. Surface Energy and the Contact of Elastic Solids. *Proc. R. Soc. Lond. A Math. Phys. Sci.* 1971, 324 (1558), 301–313.
- (28) Maugis, D. Adhesion of Spheres: The JKR-DMT Transition Using a Dugdale Model. *J. Colloid Interface Sci.* **1992**, *150* (1), 243–269.
- (29) Tabor, D. The Hardness of Solids. Rev. Phys. Technol. 1970, 1 (3), 145-179.
- (30) Tabor, D. Surface Forces and Surface Interactions. J. Colloid Interface Sci. 1977, 58 (1), 2.
- (31) Jacobs, T. D. B.; Mathew Mate, C.; Turner, K. T.; Carpick, R. W. Understanding the Tip-Sample Contact: An Overview of Contact Mechanics from the Macro- to the Nanoscale. In *Scanning Probe Microscopy for Industrial Applications: Nanomechanical Characterization*, 2013; pp 15–48.
- (32) Andreozzi, L.; Castelvetro, V.; Faetti, M.; Giordano, M.; Zulli, F. Rheological and Thermal Properties of Narrow Distribution Poly(Ethyl Acrylate)S. *Macromolecules* **2006**, *39* (5), 1880–1889.
- (33) Gao, J.; McManus, N. T.; Penlidis, A. Experimental and Simulation Studies on Ethyl Acrylate Polymerization. *Macromol. Chem. Phys.* **1997**, *198* (3), 843–859.
- (34) Krause, S.; Gormley, J. J.; Roman, N.; Shetter, J. A.; Watanabe, W. H. Glass Temperatures of Some Acrylic Polymers *J. Polym. Sci., Part A: Gen. Pap.* 3 103573 3586 DOI: 10.1002/pol.1965.100031020.
- (35) Laki, S.; Shamsabadi, A. A.; Riazi, H.; Grady, M. C.; Rappe, A. M.; Soroush, M. Experimental and Mechanistic Modeling Study of Self-Initiated High-Temperature Polymerization of Ethyl Acrylate. *Ind. Eng. Chem. Res.* **2020**, *59* (6), 2621–2630.
- (36) Huseby, T. W.; Matsuoka, S. Mechanical Properties of Solid and Liquid Polymers. *Mater. Sci. Eng.* **1967**, *1* (6), 321–341, DOI: 10.1016/0025-5416(67)90014-6.
- (37) Liu, H.; Wu, F. Y.; Zhong, G. J.; Li, Z. M. Predicting the Complex Stress-Strain Curves of Polymeric Solids by Classification-Embedded Dual Neural Network. *Mater. Des.* **2023**, 227, No. 111773.
- (38) Li, T.; Li, H.; Wang, H.; Lu, W.; Osa, M.; Wang, Y.; Mays, J.; Hong, K. Chain Flexibility and Glass Transition Temperatures of Poly(n-Alkyl (Meth)Acrylate)s: Implications of Tacticity and Chain Dynamics. *Polymer* **2021**, *213*, No. 123207.
- (39) Li, Z.; Bui, H. S. Factors Affecting Cosmetics Adhesion to Facial Skin. In *Surface Science and Adhesion in Cosmetics*; Wiley, 2021; pp 549–584.
- (40) Luengo, G. S.; Potter, A.; Ghibaudo, M.; Baghdadli, N.; Enea, R.; Song, Z. Stratum Corneum Biomechanics (Mechanics and Friction): Influence of Lipids and Moisturizers. In *Agache's Measuring the Skin: Non-invasive Investigations, Physiology, Normal Constants*, 2nd ed.; Springer International Publishing, 2017; pp 373–387.
- (41) Saldivar-Guerra, E.; Vivaldo-Lima, E. Handbook of Polymer Synthesis, Characterization, and Processing; Wiley, 2013.
- (42) Buback, M. Free-Radical Polymerization up to High Conversion. A General Kinetic Treatment. *Makromol. Chem.* **1990**, 191, 1575–1587.

- (43) Penzel, E.; Rieger, J.; Schneider, H. A. The Glass Transition Temperature of Random Copolymers: 1. Experimental Data and the Gordon-Taylor Equation. *Polymer* 1997, 38 (2), 325–337.
- (44) Metin, B.; Blum, F. D. Molecular Mass and Dynamics of Poly(Methyl Acrylate) in the Glass-Transition Region. *J. Chem. Phys.* **2006**, 124 (5), No. 054908, DOI: 10.1063/1.2162879.
- (45) Shetter, J. A. Effect of Stereoregularity on the Glass Temperatures of a Series of Polyacrylates and Polymethacrylates. *J. Polym. Sci.* **1963**, *1* (5), 209–213.
- (46) Ali, A. H.; Srinivasan, K. S. V.; Division, P. Studies on the Thermal Degradation of Acrylic Polymers by Simultaneous Autostep TG/DTA Acrylic Polymers by Simultaneous Autostep TG/DTA. *J. Macromol. Sci., Part A: Pure Appl. Chem.* 1997, 34 (2), 235–246.
- (47) Ebnesajjad, S. Adhesives Technology Handbook, 2nd ed.; 2009.
- (48) Liu, S.; Srinivasan, S.; Grady, M. Č.; Soroush, M.; Rappe, A. M. Backbiting and β -Scission Reactions in Free-Radical Polymerization of Methyl Acrylate. *Int. J. Quantum Chem.* **2014**, 114 (5), 345–360.
- (49) Yamada, B.; Kobatake, S. Radical Polymerization, Co-Polymerization, and Chain Transfer of α -Substituted Acrylic Esters. *Prog. Polym. Sci.* **1994**, *19*, 1089.
- (50) Comyn, J.; Fernandez, R. A. Glass Transition Temperatures of Copolymers of Ethyl Acrylate and Vinylidene Chloride. *Eur. Polym. J.* 1975, 11 (2), 149–151.
- (51) Odent, J.; Leclère, P.; Raquez, J. M.; Dubois, P. Toughening of Polylactide by Tailoring Phase-Morphology with P[CL-Co-LA] Random Copolyesters as Biodegradable Impact Modifiers. *Eur. Polym. J.* **2013**, 49 (4), 914–922.
- (52) Surin, M.; Hennebicq, E.; Ego, C.; Marsitzky, D.; Grimsdale, A. C.; Müllen, K.; Brédas, J. L.; Lazzaroni, R.; Leclère, P. Correlation between the Microscopic Morphology and the Solid-State Photoluminescence Properties in Fluorene-Based Polymers and Copolymers. *Chem. Mater.* **2004**, *16* (6), 994–1001.
- (53) Tong, J. D.; Leclère, P.; Doneux, C.; Brédas, J. L.; Lazzaroni, R.; Jérôme, R. Synthesis and Bulk Properties of Poly(Methyl Methacrylate)-b-Poly(Isooctyl Acrylate)-b-Poly(Methyl Methacrylate). *Polymer* **2000**, *41* (12), 4617–4624.
- (54) Dokukin, M. E.; Sokolov, I. Quantitative Mapping of the Elastic Modulus of Soft Materials with HarmoniX and PeakForce QNM AFM Modes. *Langmuir* **2012**, 28 (46), 16060–16071.
- (55) Mendoza-Muñoz, N.; Leyva-Gómez, G.; Piñón-Segundo, E.; Zambrano-Zaragoza, M. L.; Quintanar-Guerrero, D.; Del Prado Audelo, M. L.; Urbán-Morlán, Z. Trends in Biopolymer Science Applied to Cosmetics. *Int. J. Cosmet. Sci.* **2023**, 45 (6), 699–724.
- (56) Portal, J.; Garcon, R. Cosmetic Composition Comprising a Polyhydroxyalkanoate in an Oily Medium. U.S. Patent US12,257,336, 2018.
- (57) Sun, Z.; Ramsay, J. A.; Guay, M.; Ramsay, B. A. Carbon-Limited Fed-Batch Production of Medium-Chain-Length Polyhydroxyalkanoates from Nonanoic Acid by Pseudomonas Putida KT2440. *Appl. Microbiol. Biotechnol.* **2007**, *74* (1), 69–77.

